Journal of the Energy Institute 108 (2023) 101239

Contents lists available at ScienceDirect

Journal of the Energy Institute

journal homepage: www.elsevier.com/locate/joei

Co-gasification of rice husk and plastic in the presence of CaO using a novel ANN model-incorporated Aspen plus simulation

Jamilu Salisu [a,b], Ningbo Gao [a,*], Cui Quan [a], Jale Yanik [c], Nancy Artioli [d]

[a] International Joint Research Center for Solid Waste Recycling and Utilization, Energy and Power Engineering, Xi'an Jiaotong University, Xi'an, Shaanxi, 710049, China
[b] Department of Chemical Engineering, Modibbo Adama University, Yola, Nigeria
[c] Faculty of Science, Department of Chemistry, Ege University, 35100, Bornova, Izmir, Turkey
[d] DICATAM - Department of Civil, Environmental, Architectural Engineering and Mathematics, University of Brescia, Via Branze 43, Brescia, Italy

ARTICLE INFO

Handling Editor: Dr. Paul Williams

Keywords:
Co-gasification
H_2-rich syngas
CO_2 capture
Aspen plus
ANN model

ABSTRACT

This study presents a novel model for the simulation of co-gasification of rice husk and plastic using Aspen Plus. The new approach involved using an artificial neural network (ANN) to predict pyrolysis process involved in the gasification, purposely with the aim of providing a more realistic model. Three ANN models were developed with inputs as ultimate analysis (C, H and O), higher heating value (HHV) and pyrolysis temperature. In the gasification section, effects of temperature (600–850 °C), steam-to-feed ratio and CaO to feed ratio were examined. The developed ANN models proved to have good agreement with the actual data with a correlation coefficient (R) > 0.979. The performances of the models were also assessed by absolute mean error (MAE), root mean square error (RMSE) and mean bias error (MBE). A maximum of 69.42 vol% H_2 content was obtained at 750 °C from the Aspen Plus gasification model, which was validated with experimental data and a least RMSE of 2.62 was obtained.

1. Introduction

The search for alternative sources of energy is driven by the need to reduce both the global dependency on fossil fuels and its environmental issues. The concern for energy security is also accelerated by the increasing world population [1]. In addition, advancement in technology and changes in human being lifestyle means more demand for energy. On the other hand, environmental issues arise with the need to reduce greenhouse gases, especially with the usage of fossil fuels. Therefore, world policymakers continue to emphasize on renewable, clean and affordable sources of energy [2].

Recently, energy from biomass has been considered as a sustainable source of energy, which meets the above criteria. Technologies for conversion of biomass to energy are biochemical and thermochemical methods. Various types of biomass including waste such as agricultural residue and municipal waste [3] can be accommodated by the thermochemical method (combustion, pyrolysis and gasification). Among these, gasification offers additional advantages of higher efficiency and variable end-use application. Biomass gasification is the partial oxidation of organic material using gasifying agents such as pure oxygen, air, steam to produce a combination of gases known as syngas comprised mainly of H_2, CO and CH_4 [4]. Gasification of biomass together with plastic is inspired by the need to increase the H/O ratio [5] and also serves as a way of disposing plastic. Plastics are major environmental concern due to their non-biodegradability and a large amount is generated annually (400 million tonnes in 2016). Thus by the year 2030, it is estimated that about 12 billion tons of plastic could end up in landfills if not properly managed [6].

Syngas is the main product of gasification, but generated along are char (unconverted carbon and ash), tar (higher condensable hydrocarbons) and CO_2 as impurities. Syngas can be used for heating, electricity and chemicals production. To capture CO_2 and increase H_2 content in the syngas, sorbent such as CaO is employed in sorption-enhanced gasification. This, together with the use of steam as a gasifying agent produces H_2-rich syngas with low CO_2, guided by Le Chatelier's principle which enhances water-gas shift reaction. In addition, the presence of CaO also promotes tar cracking and tar reforming [7].

Mathematical modelling or simulation is employed to design or optimize complex processes such as gasification. Simulation eliminates the time constraints by providing necessary preliminary information such as economic and technical feasibility of a process. Among these models are thermodynamic equilibrium models, which are independent

* Corresponding author.
E-mail address: nbogao@xjtu.edu.cn (N. Gao).

https://doi.org/10.1016/j.joei.2023.101239
Received 17 November 2022; Received in revised form 15 March 2023; Accepted 21 March 2023
Available online 22 March 2023

Table 1
Ultimate and proximate properties of the feed.

Ultimate Analysis (dry basis)			Proximate Analysis			HHV[d] (MJ/kg)	
(wt%)	RH	LDPE	(wt%)	RH	LDPE	RH	LDPE
C	41.61	83.49	Moisture	9.18		15.90	47.66
H	5.57	14.07	Volatile matter	63.03	99.99		
N	1.08	0.03	Fixed carbon[a]	6.48			
S	0.05	0.02	Ash	21.31			
O[a]	51.69	2.39					

[a] Calculated by difference.
[d] calculated using Dulong's formula.

of the reactor (gasifier) design. Hence, they are convenient to apply through either the chemical equilibrium constant or minimization of Gibbs's free energy approach. Many works have developed equilibrium models to simulate steam gasification of biomass in the presence of CaO with CO_2 capture using Aspen Plus model [8–11]. However, these equilibrium models have the limitation of over-prediction of H_2 and CO contents and under-prediction of CO_2 and CH_4. Unfortunately, none of the previous studies involving sorption-enhanced gasification using Aspen Plus simulation has considered modifying the equilibrium model. Although some studies involving different gasification technology have used some modified equilibrium models [12–15].

Basically, these modified models focused on two approaches [16]: (i) use of modified equilibrium temperature to restrict some reactions, (ii) use of experimental empirical relation. However, some of the modified models do have their limitations, for instance, Fernandez-Lopez et al. [17] assumed that some key reactions happened at a lower temperature than the normal gasification temperature.

In addition, gasification involves a pyrolysis process and most studies [8,18,19], model the pyrolysis process by using fractional yield based on the feed's ultimate analysis. However, this does not represent the actual pyrolysis products (char, liquid and gases), as such tar is neglected [8, 10,18]. Hence, the idea in this study is to model the pyrolysis stage using an artificial neural network (ANN) separately and incorporating it into an Aspen Plus model using a modified equilibrium model approach. This will give a more realistic model using ANN pyrolysis products derived from experimental data. Although, some studies [20,21] have used correlation to predict the pyrolysis products using only temperature as the regression input parameter. Here, ultimate analysis (C, H and O), higher heating value (HHV) and temperature are used as the input parameters. Thus, co-gasification of rice husk (RH) and low-density polyethylene (LDPE) is considered in this study in the presence of CaO using an ANN-incorporated Aspen Plus simulation. ANN is a computational model technique that is inspired by the function and structure of the human brain. Using this concept of neurons, ANN modelling does not require a mathematical description of the process [22]. Thus, making ANN a powerful and accurate method used in numerical prediction such as gasification where complex nonlinear relationship between output and input parameters exist [23]. ANN is considered newest among its counterpart for modelling [24], but due to its flexibility, ANN has been successfully used for prediction of many thermochemical processes. These include; pyrolysis of pine sawdust prediction [25], tar prediction [26], prediction of kinetic parameters of pyrolysis [27], gasification in a fixed bed [28,29], gasification in fluidized bed [30,31], gasification in an entrained gasifier [32], sorption-enhanced gasification [33], combustion [34]. Recently, Safarian et al. [22] developed a hybrid model with Aspen Plus and ANN, in which, gasification is modelled using Aspen Plus simulation. ANN on the other hand was used to predict power generation resulting from the gasification.

2. Materials and methods

2.1. Sample characterization

Rice husk was obtained from Nigeria and LDPE powder was purchased from Baoji Guokang Bio-Technology, China. As shown in Table 1, their ultimate analyses were determined using a CHN-elemental analyzer. Their proximate analyses were determined according to ASTM D3302-07a, ASTM D3175-89a and NREL/TP-510- 42622 procedures, respectively for moisture content, ash and volatile matter.

2.2. ANN model development

The basic processing unit of ANN is called "neuron or perceptron" which interconnects input and output data. Activation function then

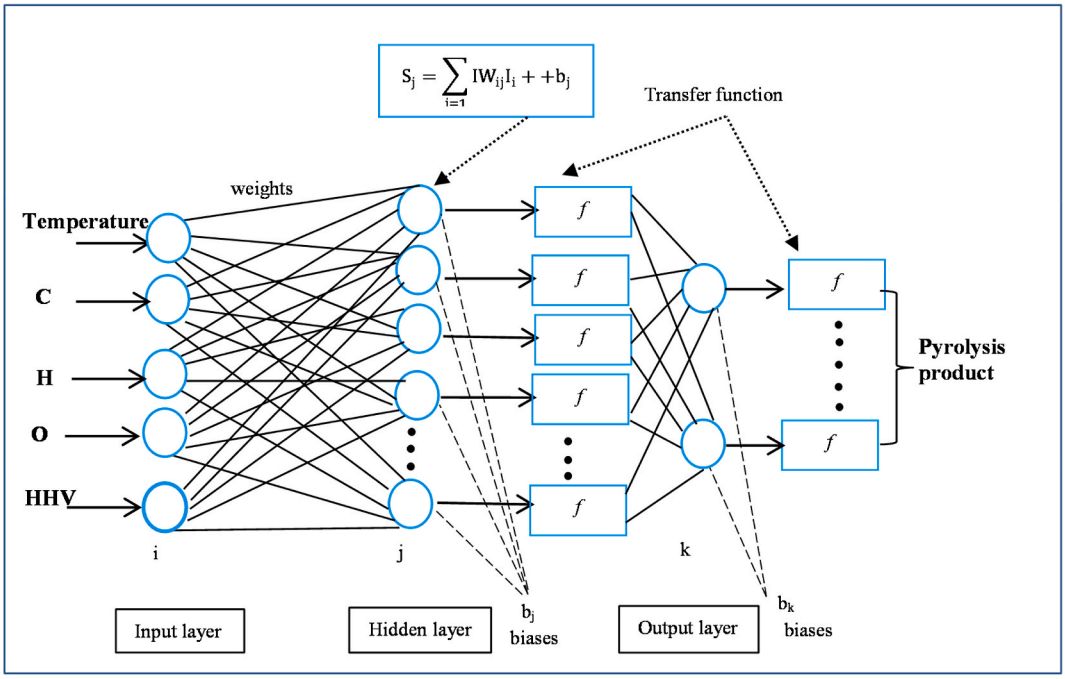

Fig. 1. Architecture of the ANN model used in this study.

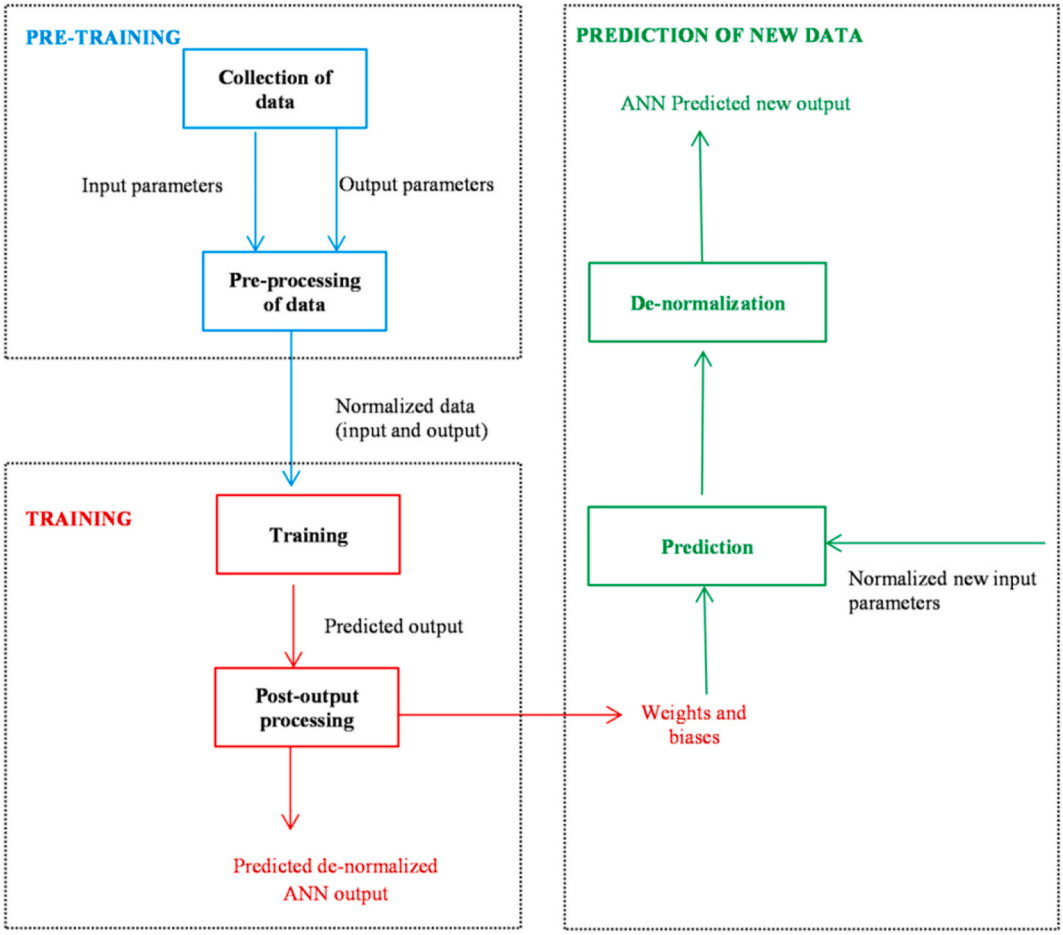

Fig. 2. ANN model developing process.

propagates the data from one layer to the other using a non-linear equation. As such, an ANN model structure consists of three layers; input, hidden and output layers. The hidden layer receives sum of weighted input from an external source (input layer) [35].

In this study, three ANN models were developed; model 1: prediction of biomass pyrolysis products, model 2: prediction of plastic pyrolysis products and model 3: prediction of gas composition. The data sets used in the development are 98, 56 and 59, respectively for models 1, 2 and 3 (see supplementary data). The input parameters for all the models consist of 5 neurons as pyrolysis temperature, ultimate analysis (C, H and O) and higher heating value (HHV). For the hidden layer, 5–12 neurons were selected and varied based on trial and error method to obtain the best structure. For both ANN models 1 and 2, the output layers contained two neurons as pyrolysis products yields of gas and liquid, while char = 100% - (gas + liquid). For ANN model 3, three neurons as H_2, CH_4 and CO are contained in the output layers as gas composition, while $CO_2 = 100$- (H_2, CH_4 and CO). The ANN architecture used in developing the models is shown in Fig. 1.

Each model is trained in the Neural Network Toolbox (nntool) of MATLAB environment (R2018a). Feed forward-multi-layer perception (MLP) approach is used to develop the ANN models using Levenberg–Marquardt (LM) backpropagation algorithm (TRAINLM). In addition, gradient descent with momentum weight and bias (LEARNGDM) is adapted as the learning function. LM algorithm is considered the fastest and stable algorithm, which combines two minimization techniques such as Gauss-Newton and gradient-descent methods [36]. The algorithm is also suitable for small-size ANN structure [31]. To obtain the best model, a different combination of activation functions of hyperbolic tangent sigmoid (tansig) and linear function (purelin) were chosen in both hidden and input layers. Tansig transforms data in the ranges of −1.0 and 1.0. The equation of the tangent sigmoid function is given as:

$$f(x) = \frac{e^{x} - e^{-x}}{e^{x} + e^{-x}} \tag{1}$$

Before and after the training, ANN normalizes input data and de-normalizes output data according to Equations (2) and (3), respectively [37].

After developing the models, using Equation (4) [38] and the weights and biases generated from the trained ANN models, pyrolysis products of new inputs are predicted. As described in Fig. 2, the new input here refers to the feed materials (RH and LDPE) presented in Table 1, which are used in the Aspen Plus simulation.

$$Y_k = \left(\frac{y_k + 1}{2}\right)(y_{max} - y_{min}) + y_{min} \tag{2}$$

$$X_i = 2\left(\frac{X_i - X_{min}}{X_{max} - X_{min}}\right) - 1 \tag{3}$$

$$Y_k = tansig\left[b_{2k} + \sum_{j=1}^{m}\left[\mathrm{JW_{jk}} \times \mathrm{tansig}\left(\mathrm{b_{1j}} + \sum_{i=1}^{n} \mathrm{IW_{Ij}} X_i\right)\right]\right] \tag{4}$$

Y_k is the predicted de-normalized output parameter of the pyrolysis product and X_i is the normalized input parameter, X_{min}/Y_{min} and X_{max}/Y_{max} represent the minimum and maximum values within the scaling ranges, respectively.

$IW_{j,I}$ and b_1 are the weights and biases connecting between Ith input layer and jth hidden layer, respectively. While, $JW_{k,j}$ and b_2 represent

weights and biases connecting jth hidden layer and kth output layer, respectively, n and m are the number of neurons in the input and hidden layers, respectively.

2.2.1. Performance evaluation of ANN models

The performances of the different developed ANN models are assessed by the following parameters:

$$\text{Correlation coefficient (R)} = \frac{\frac{1}{n}\sum_{i=1}^{n}((A_i - \overline{A})(P_i - \overline{P}))}{\sqrt{\sum_{i=1}^{n}(A_i - \overline{A})^2 \sum_{i=1}^{n}(P_i - \overline{P})^2}} \quad (5)$$

$$\text{Root mean square error (RMSE)} = \sqrt{\frac{\sum_{i=1}^{n}(A_i - P_i)^2}{n}} \quad (6)$$

$$\text{Mean absolute error (MAE)} = \frac{1}{n}\sum_{i=1}^{n}|A_i - P_i| \quad (7)$$

$$\text{Mean bias error (MBE)} = \frac{1}{n}\sum_{i=1}^{n}(A_i - P_i) \quad (8)$$

Where A_i stands for actual values, P_i is the predicted values and n represents the size of data.

2.3. Gasification using aspen plus simulation

2.3.1. Model assumptions

In this model, the assumptions considered are outlined below:

- An isothermal and steady-state process is assumed with uniform atmospheric pressure throughout.
- Ash is considered inert in the gasification process.
- Redlich-Kwong-Soave with Boston-Mathias (RKS-BM) alpha function equation is used to estimate the properties of the gases involved.
- Primary pyrolysis products of rice husk are gases (CO_2, CO, CH_4, and H_2), char (ash and carbon) and tar contains mainly oxygenates, which are represented by $C_2H_4O_2$ and C_6H_6O [39,40].
- Primary pyrolysis products for LDPE are gases (C_2H_4 and C_3H_6), char (carbon) and tar contains mainly alkenes and alkane, which are represented by $C_{10}H_{20}$ and $C_{16}H_{34}$ [41,42].
- The cleaning unit is not modelled in detail and sulfur and nitrogen are not taken into consideration [43].

2.3.2. Physical property method

Before starting a simulation in Aspen Plus, property and method must be chosen. Here, a stream class of MIXCINC is specified, meaning both conventional substances and nonconventional solids are involved. A non-conventional solid component is recognized by Aspen Plus as a substance characterized using empirical factors known as component attributes, which are represented by their component composition. These types of substances are not involved on their own in phase and chemical equilibrium. Both RH and LDPE are considered nonconventional solids, which are inputted according to their ultimate and proximate analyses, HCOALGEN and DCOALIGT are used to evaluate their density and enthalpy respectively. In this simulation, RKS- BM (RK-Soave equation) property method was chosen, which is recommended for gas-processing and refinery/petrochemical under high temperatures and many works have recorded convincing results for gasification process [12,44–46].

2.3.3. Aspen plus model development

Gasification process involves three main stages as drying, pyrolysis and reduction/oxidation. Drying reduces the moisture of the feed to <5 wt% [43] at 100–200 °C with no chemical reaction taking place.

Table 2
Main reactions involved in a gasification process.

Reaction name	Chemical reaction	ΔH (kJ/mol)	Reaction I.D
Boudouard	$C + CO_2 \longrightarrow 2CO$	+172 kJ/mol	R1
Char gasification	$C + H_2O \longrightarrow CO + H_2$	+131 kJ/mol	R2
Methanation	$C + 2\ H_2 \longrightarrow CH_4$	−74.8 kJ/mol	R3
Water-gas shift	$CO + H_2O \longrightarrow CO_2 + H_2$	−41.2 kJ/mol	R4
Steam reforming	$CH_4 + H_2O \longrightarrow CO + 3H_2$	+206 kJ/mol	R5
Carbonation	$CaO + CO_2 \longrightarrow CaCO_3$	−178 kJ/mol	R6

Pyrolysis involves thermal decomposition (devolatilization) of the dry solid component in the absence of oxygen at 200–700 °C into volatiles (gases) components, tar (liquid) and char (solid). In reduction/oxidation stage, various chemical reactions occur, prominent among (Table 2) them are the Boudouard reaction (R1) water-gas shift reaction (R4) and water-gas (R4), this stage determines the final composition of syngas. In Aspen Plus simulation, these stages are represented in different units.

This simulation was carried out using Aspen Plus V9 software. The feed stream comprises of mass flow of 80 kg/h RH and 20 kg/h LDPE, which are fed to the gasification system, as RICEHUSK and LDPE, respectively. At the feed ratio of 8:2 (RH: LDPE), it is assumed that 20% of LDPE comes from waste around a real RH gasification plant [47]. As shown in Fig. 3 and Table 3, only RH undergoes drying process, since moisture content of LDPE is very low. A stoichiometric reactor, DRYING is used for the drying process at 150 °C. A calculator block with a Fortran statement is utilized to control the amount of water, RH-H20 to be evaporated, the extent of the drying is specified as 5% [43]. A separator, SEP1 separates the evaporated water, DRYH2O from the DRIEDRH, which then goes to the pyrolysis unit PYR1, while PYR2 is utilized for pyrolysis of LDPE. The pyrolysis process is modelled using the RYield reactor at 500 °C. At this stage, the feeds are decomposed into their corresponding gases, tar and char, according to the yields obtained from the ANN model results in section 3.1. Tars are separated from other pyrolysis products as PYRRH2 and PYRLD2 in SEP2 and SEP3 and cracked to gases and secondary tars in TARC1 and TARC2 [20], respectively for RH and LDPE. Here, as described by Equations (9)–(12), the primary tars are $C_{10}H_{20}$ and $C_{16}H_{34}$ for RH and $C_2H_4O_2$ and C_6H_6O for LDPE, the secondary tars are $C_{10}H_8$, C_6H_6, and CH_2CO.

$$C_6H_6O \longrightarrow 0.4C_{10}H_8 + 0.15C_6H_6 + 0.1CH_4 + CO + 0.75H_2 \quad (9)$$

$$CH_3COOH \longrightarrow CH_2CO + H_2O \quad (10)$$

$$C_{16}H_{34} \longrightarrow 2C_2H_4 + 4C_2H_2 + 4CH_4 + H_2 \quad (11)$$

$$C_{10}H_{20} \longrightarrow 2C_2H_4 + 2C_2H_2 + 2CH_4 \quad (12)$$

After the cracking, SEP4 further separates RH secondary tar from other cracking products. It is assumed that 4.5% [48], PYRLD5 of the RH secondary tar is unconverted (will not undergo steam reforming), this is done with SLIT. The final pyrolysis and cracking products are then mixed in MIXER1 and MIXER2. Before undergoing gasification with STEAM1 (200 °C) in GASIF1 using an RGibbs reactor, which assumes chemical equilibrium according to the minimizing of Gibbs energy approach, here temperature is varied between 600 and 850 °C. Products, GASIF1P from the GASIF1 are passed to the GASIF2 under the same reaction conditions. In the GASIF2, sorbent-enhanced gasification occurs using CaO at a flow of 100 kg/h, according to reaction R6, in this reactor also, a modified equilibrium factor is applied. Where, water-gas shift reaction (R4) and reversed steam reforming reaction (R5) are restricted [49], occurring at 0.6 fractional conversion of CO and 0.2 conversion of H_2, respectively. After the gasification, raw syngas is passed to FILTER, SSEP and SEP5 to remove char/ash (ASH), $CaCO_3$/unreacted CaO (CACO3) and tar/water (BY-PROD), respectively. Finally, PURESYN stream is obtained, which contained syngas with a composition of H_2, CO, CH_4 and CO_2.

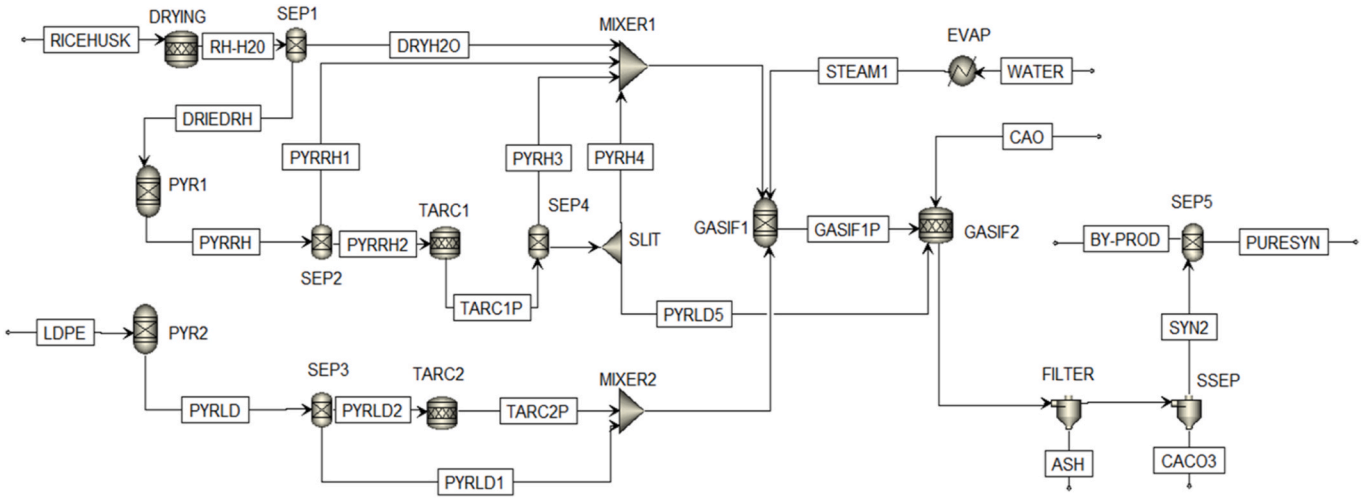

Fig. 3. Flowsheet describing Aspen plus simulation of the co-gasification process.

Table 3
Description of various units of the Aspen Plus model.

Block I.D.	Aspen Plus model name	Description
DRYING	RStoic	Reduce moisture content of RH using defined stoichiometric reaction
SEP1	Sep2	Separate dried RH from water
PYR1& PYR2	RYield	Convert non-conventional feed into their constituent pyrolysis components at 500 °C and 1 atm according to the ANN model results
SEP2 & 3	Sep2	Separate tars from other pyrolysis components
TARC1 & TARC2	RStoic	Simulate cracking of primary tar into lighter molecules and secondary tar at 600–850 °C and 1 atm
SEP4	Sep2	Separate produced secondary/primary tars from gases
SLIT	SPLIT	Split separated tar from SEP4 into converted (PYRRH4) and unconverted (PYRRH5)
MIXER1 & 2	Mixer	Mix the final pyrolysis products
EVAP	Heater	Generate steam at 200 °C and 1 atm
GASIF1	RGibbs	Simulate steam gasification according to the Gibbs minimization of energy approach at 600–850 °C and 1 atm
GASIF2	RStoic	Sorbent enhanced gasification and modification of equilibrium model at 600–850 °C and 1 atm
FILTER	SSplit	Separate ash and char from the gasification products
SSEP	SSplit	Separate $CaCO_3$/CaO from the gasification products
SEP5	Sep2	Separate by-products from syngas

2.3.4. Gasification performance evaluation

The performance of the gasification is measured by the composition of syngas: H_2, CO, CH_4 and CO_2. Also assessed by gas yield, Nm^3/kg, lower heating value of the syngas (LHV_{gas}), MJ/Nm^3 [12], cold gas gasification efficiency (CGE) and carbon conversion efficiency (CCE), these given by equations (13)–(16), respectively.

$$\text{Gas yield} = \frac{Q_{gas}}{m_{feed}} \tag{13}$$

$$LHV_{gas} = 10.8{*}yH_2 + 12.6 * yCO + 35.8 * yCH_4 \tag{14}$$

$$CGE = \frac{LHV_{gas} * Q_{gas}}{m_{feed} * LHV_{feed} + m_{steam} * H_{steam}} \tag{15}$$

$$CCE = \frac{12 * GY(CO\% + CO_2 + CH_4)}{24 * C\%} \tag{16}$$

where Q_{gas} is the total syngas produced (Nm^3), m is mass flow (kg/hr), H_{steam} is the steam enthalpy (MJ/kg), C% is the carbon mass fraction and CO, CO_2 and CH_4 are the mole fraction of the syngas.

2.4. Experimental gasification

The experimental set-up as described in Fig. 4, consists of a vertical reactor, gas cooling/collection unit and an offline gas analyzer. The reactor is made of stainless steel with an inner diameter of 60 mm and length of 100 mm. Basket containing mixed samples of feedstock and CaO is placed 15 mm away from the top of the reactor. After loading, each experiment proceeds with heating in 50 mL/min N_2 flow. Steam with N_2 flow of 50 mL/min is charged when the temperature reached 200 °C and the heating continued until the desired temperature is reached. Products from the gasification are passed through flowing water for cooling with an ice-cold trap for residual liquid (water and tar) collection. Non-condensable gases are collected using gasbag, each experiment lasted for 60 min. The collected gases are sampled for analysis using an offline gas analyzer (RGA, Agilent 7890A), equipped with one FID and two TCD detectors.

3. Results and discussion

3.1. ANN model results

It is important to consider different structures in determining the best model, thus the performances of different ANN structures are presented in Table 4. In all of the developed models, the best model is found with the structure ANN-1, which has 10 neurons in its hidden layer and tansig in both of its hidden and output layers. Tansig is a good non-linear transfer function for complex models, in which convincing results are obtained, especially for the hidden layer [22,24,37,50–52].

The R values of 0.979, 0.998 and 0.989 were found for ANN models 1, 2 and 3, respectively, in addition, their parity plots are shown in Fig. 5. In each of the models, it is observed that structures with the highest R values are with the lowest values of RSME and MAE. This is because R as a parameter measures how close the actual and the predicted values are. R values are assessed between −1 and 1, a value of 1 indicates a strong correlation, a −1 value points to a negative correlation [53]. Zeroes as R value indicate no relationship existing between the actual and the predicted values. Thus, the higher the R value, the less error in terms of RMSE and MAE.

Analyzing the inter-model performance, model 2 has the best R value of 0.998, but model 3 has the least RMSE and MAE values of 1.148 and

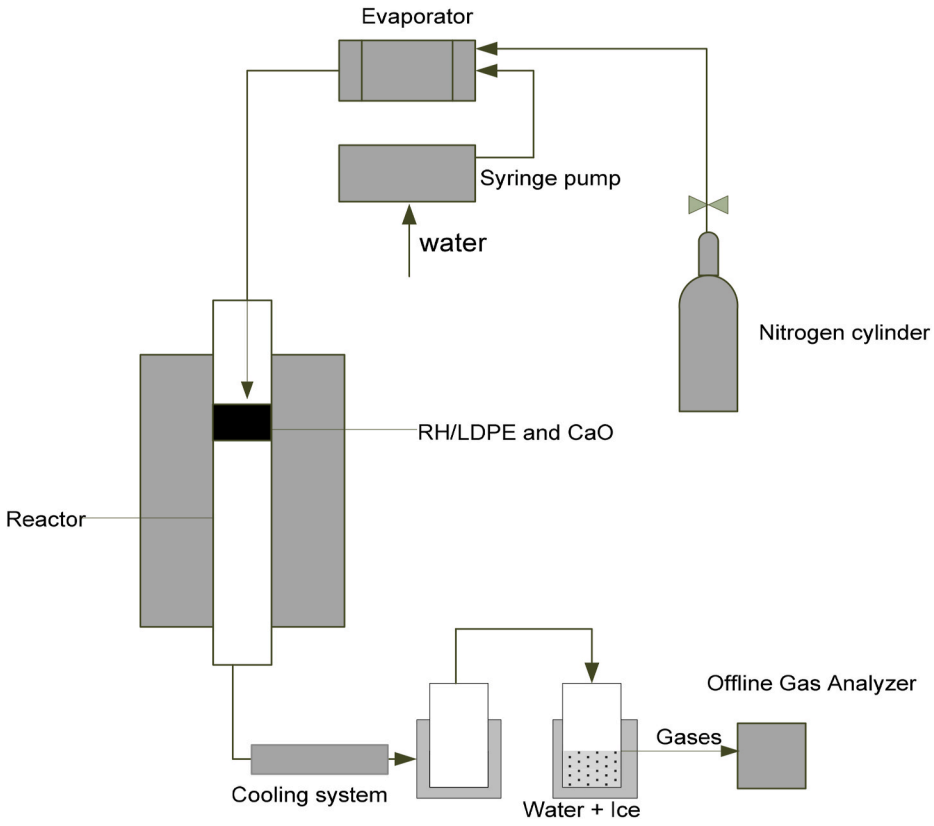

Fig. 4. Schematic representation of the experimental co-gasification.

Table 4
Performance of different ANN structures for prediction of biomass pyrolysis products (model 1), plastic pyrolysis products (model 2) and biomass pyrolysis gases (model 3).

ANN model	Structure	Network	Transfer Function		R	MAE	RSME	MBE
			Hidden layer	Output layer				
Model 1	ANN-1	5-10-2	tansig	tansig	0.979	1.639	2.247	0.074
	ANN-2	5-5-2	tansig	tansig	0.942	2.588	3.688	0.212
	ANN-3	5-12-2	tansig	tansig	0.973	1.728	2.474	0.291
	ANN-4	5-10-2	purelin	purelin	0.903	3.332	4.762	−0.184
	ANN-5	5-10-2	tansig	purelin	0.978	1.432	2.300	0.130
Model 2	ANN-1	5-10-2	tansig	tansig	0.998	1.638	2.207	0.142
	ANN-2	5-5-2	tansig	tansig	0.994	2.475	3.761	−0.147
	ANN-3	5-12-2	tansig	tansig	0.997	1.929	2.556	−0.083
	ANN-4	5-10-2	purelin	purelin	0.961	6.993	9.420	0.239
	ANN-5	5-10-2	tansig	purelin	0.995	2.619	3.572	0.147
Model 3	ANN-1	5-10-2	tansig	tansig	0.989	1.148	1.992	0.196
	ANN-2	5-5-2	tansig	tansig	0.980	1.649	2.787	0.184
	ANN-3	5-12-2	tansig	tansig	0.959	2.080	3.963	0.242
	ANN-4	5-10-2	purelin	purelin	0.942	2.707	4.680	0.022
	ANN-5	5-10-2	tansig	purelin	0.976	2.059	3.135	0.483

1.992, respectively. This can be explained by considering the average input data sets for each model, which are 15.82% gas, 80.68% liquid and 48.25% overall for model 2, as against 0.88% H_2, 4.83% CH_4, 28.14% CO and 11.28% overall for model 3. Clearly, compared to model 3, the large error of model 2 is due to its higher input values. Using MAE interpretation, it means averagely the prediction error of model 2 is 1.638, on the overall average data input of 48.25%. For model 3, MAE is 1.148 on the overall average data input of 11.28%. On the other hand, MBE as a parameter show only on average how a model is under-estimating or overestimating its prediction [54]. By this criterion, all the models overestimated their predictions with values of 0.074, 0.142 and 0.196, respectively for models 1, 2 and 3. In a similar ANN model developed by Dubdub and Al-Yaari [52], values of R, MAE and MBE were found as 0.9999, 0.1979 and −0.0048, respectively. The model was developed based on Levenberg–Marquardt algorithm for predicting char yields of different polymer pyrolysis. In the hidden layers, 10/15 neurons and TANSIG as transfer functions were found as the best parameters.

Overall, the three developed ANN models showed good agreement between the predicted and actual values. The models can be used for predicting pyrolysis products of new data inputs consisting of biomass or plastic.

3.1.1. Application of developed ANN models for prediction of new inputs

The ANN models were developed basically with the aim of using them for predicting the pyrolysis products of new input parameters and

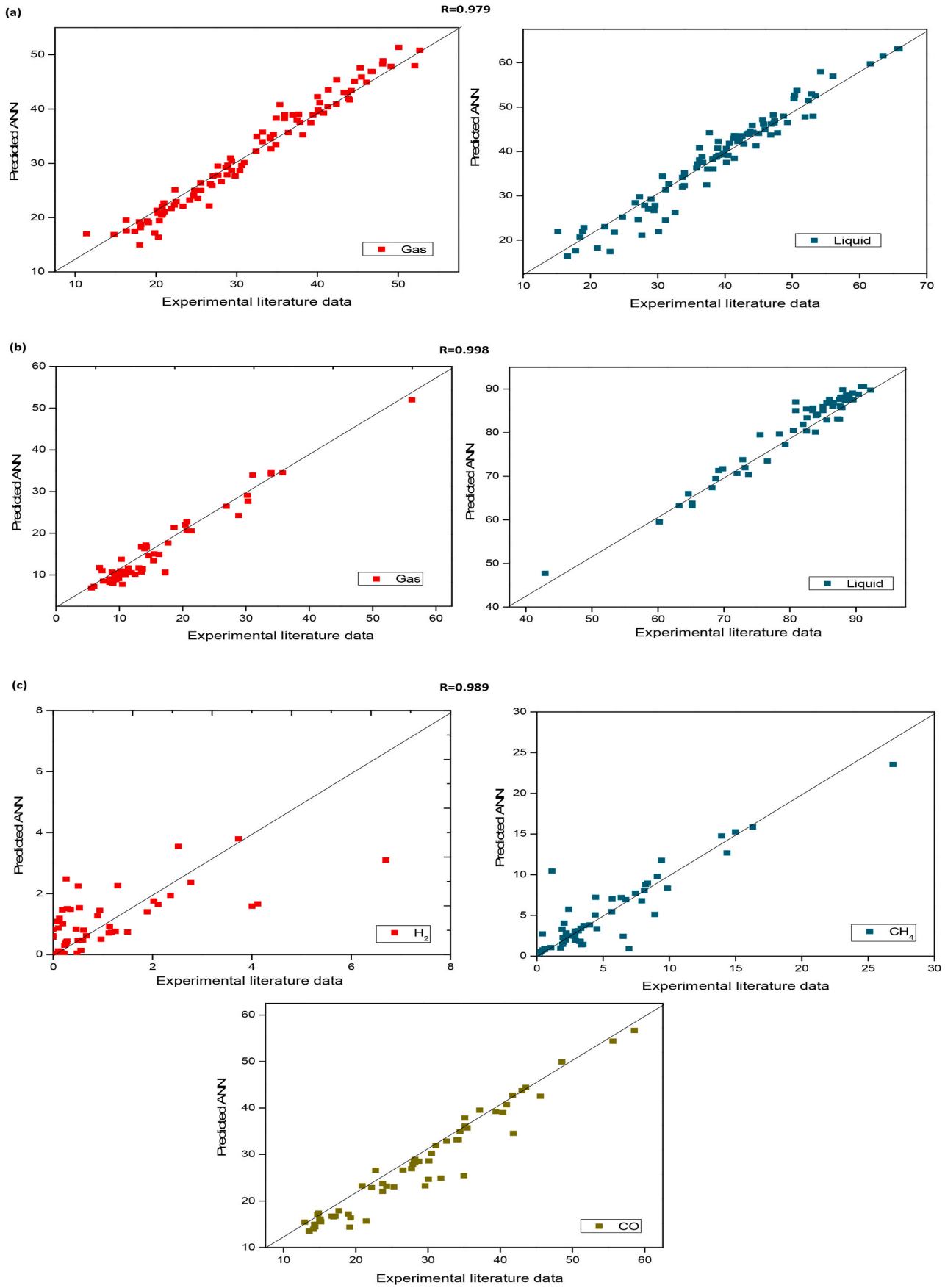

Fig. 5. Parity plots of ANN predicted result versus experimental data for (a) model 1 (biomass pyrolysis) (b) model 2 (plastic pyrolysis) (c) model 2 (biomass pyrolysis gases).

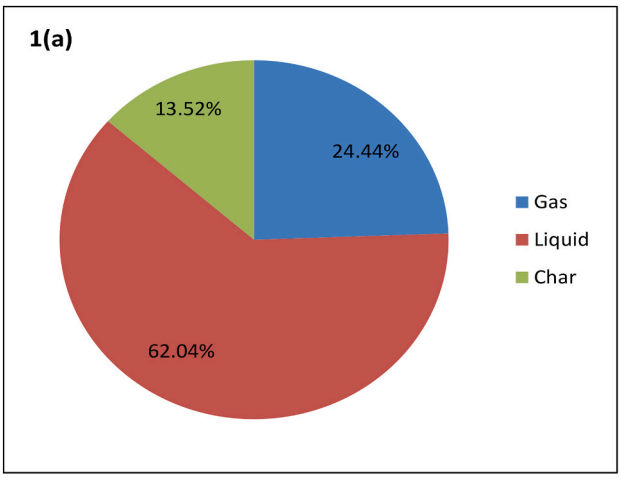

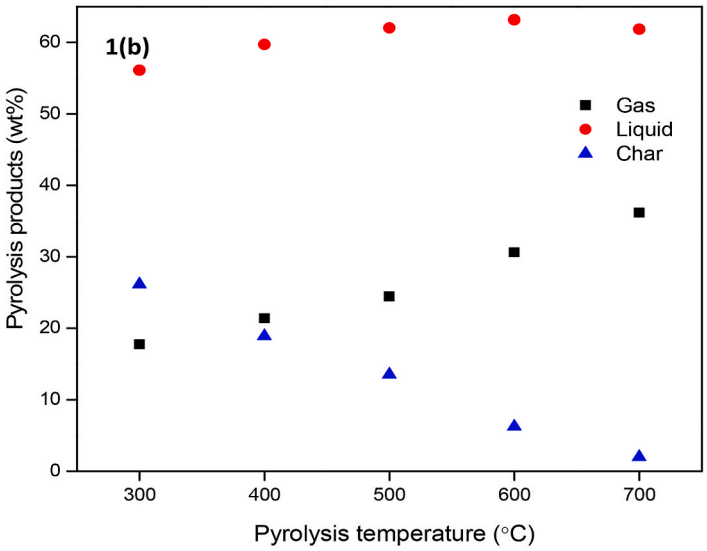

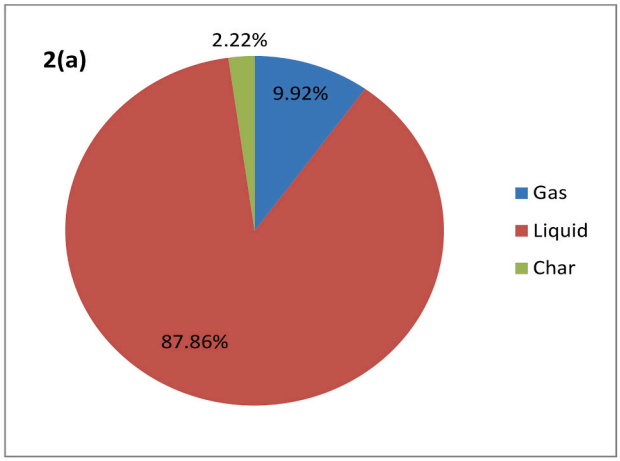

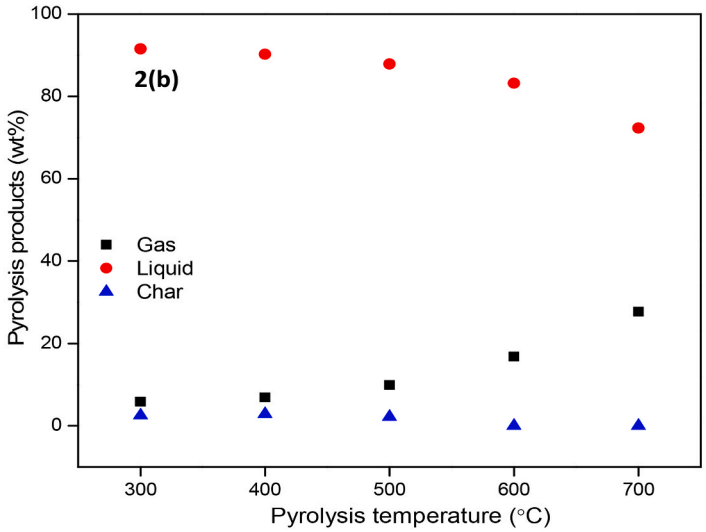

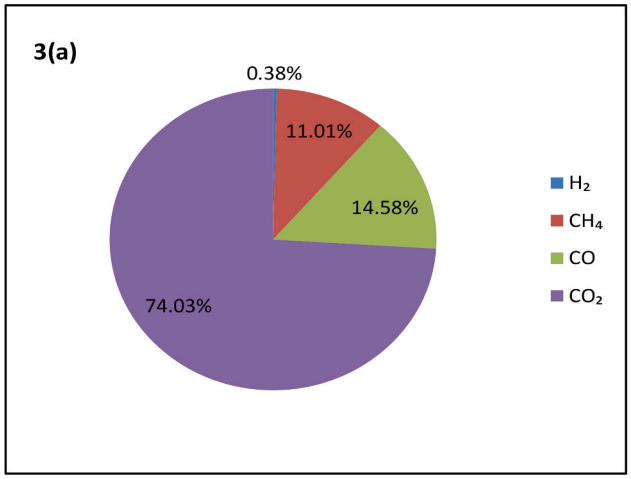

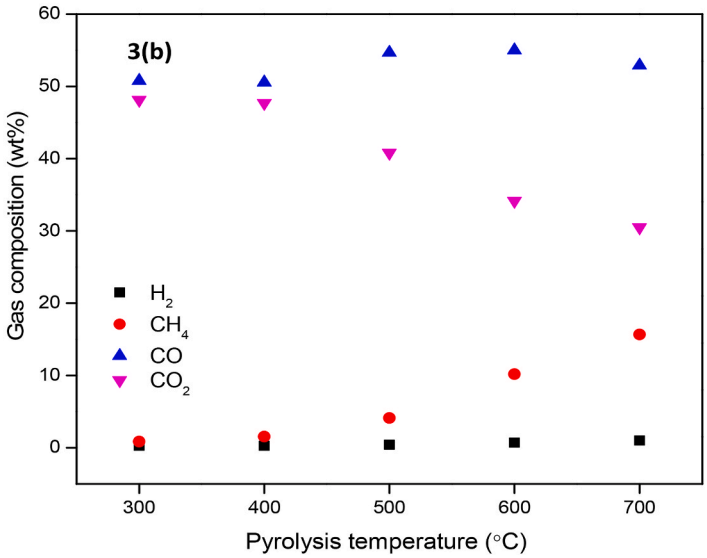

Fig. 6. ANN predicted pyrolysis product yields (wt%) for (1) rice husk (2) LDPE (3) gas composition of RH at (a) 500 °C: used in the Aspen Plus simulation (b) different pyrolysis temperature.

Table 5
Obtained ANN model weights and biases connecting input layer to hidden layer.

	Neuron	IW_{ij}					Biases
		T	H	C	O	HHV	b_{1j}
Model 1	1	−0.466	−0.524	−0.833	−3.388	−0.122	1.056
	2	−2.877	1.843	1.033	0.162	−1.823	1.422
	3	−0.213	3.551	2.080	−0.880	−0.626	−1.462
	4	−0.691	3.836	2.893	−1.596	1.948	−0.392
	5	0.055	0.664	1.887	−1.146	−2.886	−0.735
	6	−0.397	−0.756	−1.180	−2.722	1.510	−2.448
	7	−0.784	0.393	1.833	−1.614	−3.592	−1.865
	8	−0.063	2.637	−0.556	0.177	−1.912	−0.005
	9	−0.197	−2.926	−1.463	1.995	−1.533	−3.323
	10	−0.920	−0.568	−0.652	−1.041	0.903	−1.191
Model 2	1	−0.609	3.038	0.850	−2.367	−1.233	−2.813
	2	−0.299	0.409	−2.208	2.262	1.151	1.444
	3	−0.094	−0.357	−0.371	−3.512	0.655	0.480
	4	0.454	0.749	0.446	−2.761	0.083	−2.195
	5	−0.585	3.033	1.020	−0.452	1.721	−1.299
	6	0.003	3.395	9.381	−4.009	9.908	0.436
	7	−0.609	3.038	0.850	−2.367	−1.233	−2.813
	8	−0.299	0.409	−2.208	2.262	1.151	1.444
	9	−0.094	−0.357	−0.371	−3.512	0.655	0.480
	10	0.454	0.749	0.446	−2.761	0.083	−2.195
Model 3	1	−0.136	−0.134	−2.058	−3.460	−3.676	−2.025
	2	0.905	−0.132	0.282	0.812	2.357	1.888
	3	1.670	−0.694	2.613	2.210	−0.313	−0.015
	4	−0.434	−1.992	1.058	1.495	2.485	1.160
	5	0.534	1.823	−0.196	0.024	1.577	−0.624
	6	−1.438	−4.021	−0.051	−1.077	2.863	0.367
	7	1.298	3.627	1.491	−2.685	−2.474	0.803
	8	−0.315	2.202	1.542	4.881	−3.462	−1.200
	9	1.778	1.106	−1.370	−0.370	−1.107	1.590
	10	−0.448	1.513	−1.889	1.583	4.360	−2.776

Table 6
Obtained ANN model weights and biases connecting hidden layer to output layer.

	Neu ron	LW_{jK}										Biases (b_{2k})
Model 1	1	0.297	−0.552	−2.390	1.609	2.105	2.348	−1.209	1.240	0.915	−0.268	1.067
	2	−2.213	0.816	4.024	−2.525	−3.486	−1.028	1.384	−1.455	−2.605	−1.901	−1.294
Model 2	1	1.804	2.425	−1.076	−1.532	3.579	3.404	0.046	−1.591	−4.535	4.684	−1.251
	2	−2.005	−2.365	1.308	−1.088	−3.481	−0.239	1.010	1.665	3.636	−5.198	0.280
Model 3	1	−0.140	0.214	0.851	−0.850	−1.534	−1.388	−0.541	−0.715	−0.449	0.903	−0.425
	2	2.612	1.296	0.106	1.556	2.228	−2.102	−2.039	0.184	0.049	−1.620	−0.826
	3	2.899	1.049	2.572	1.992	−5.065	−2.168	1.457	−4.314	−1.148	1.911	1.384

used it in Aspen Plus gasification simulation. To do this, the optimized weights and biases for the three developed ANN models are obtained and are shown in Tables 5 and 6.

Subsequently, the pyrolysis product of RH and LDPE with the new inputs as the ultimate analysis in Table 1 are predicted and shown in Fig. 6. At 500 °C, the pyrolysis product yields of RH is 24.44% gas, 62.04% liquid and 13.52% char, while 0.41% H_2 4.11% CH_4, 54.66% CO, 40.82% CO_2 as the gas composition. Similarly, for LDPE, the pyrolysis products yields are 9.92% gas, 87.86% liquid and 2.22% char. Observably, from Fig. 6, as the pyrolysis temperature increases between 300 and 700 °C, the gas yield also increased, while the char yield decreases within the trend. This conforms to some literature [55–57] and can be explained by the fact that more solids are decomposed with the increased in temperature. For the gas composition, H_2 and CH_4 yields increase with the increase in pyrolysis temperature [56–59], H_2 is mainly from the cracking of volatile matter and CH_4 is from both depolymerization and cracking reactions [56]. Also, within the trend, noticeably is the consumption of CO_2, which is due to the Boudouard reaction.

3.2. Model validation

To test the accuracy of the developed model, the simulation data is compared with experimental data under similar conditions and RMSE was employed for the evaluation.

The RMSE results are shown in Fig. 7, with values in the order of $7.34 < 2.83 < 2.61$ for validation data sets of 600 °C, 800 °C and 700 °C, respectively at CaO/F ratio = 1 and steam/feed ratio = 1. Validation at 700 °C gives the best RMSE. As observed overall, the error contributions of H_2 and CO are the highest, while CH_4 has the least error contribution. In all, the model demonstrated good agreement with the experimental data. In addition, as presented in Fig. 8, the model is compared with that developed using the methodology by Salisu et al. [47]. As observed, with the current model, under-prediction of CH_4 and over-prediction of CO is minimized.

3.3. Effect of process parameters on gasification

3.3.1. Temperature

In gasification, temperature plays a vital role in determining the quality of syngas produced, mainly due to the complex nature of gasification involving several reactions of which some are endothermic and others are exothermic. Subsequently, gasification temperature was varied between 600 and 850 °C, at CaO/F ratio = 1 and steam/feed ratio = 1, as shown in Fig. 10. Observably, as the temperature increases, H_2 content also increases up to a maximum point of 69.42 vol% at 750 °C.

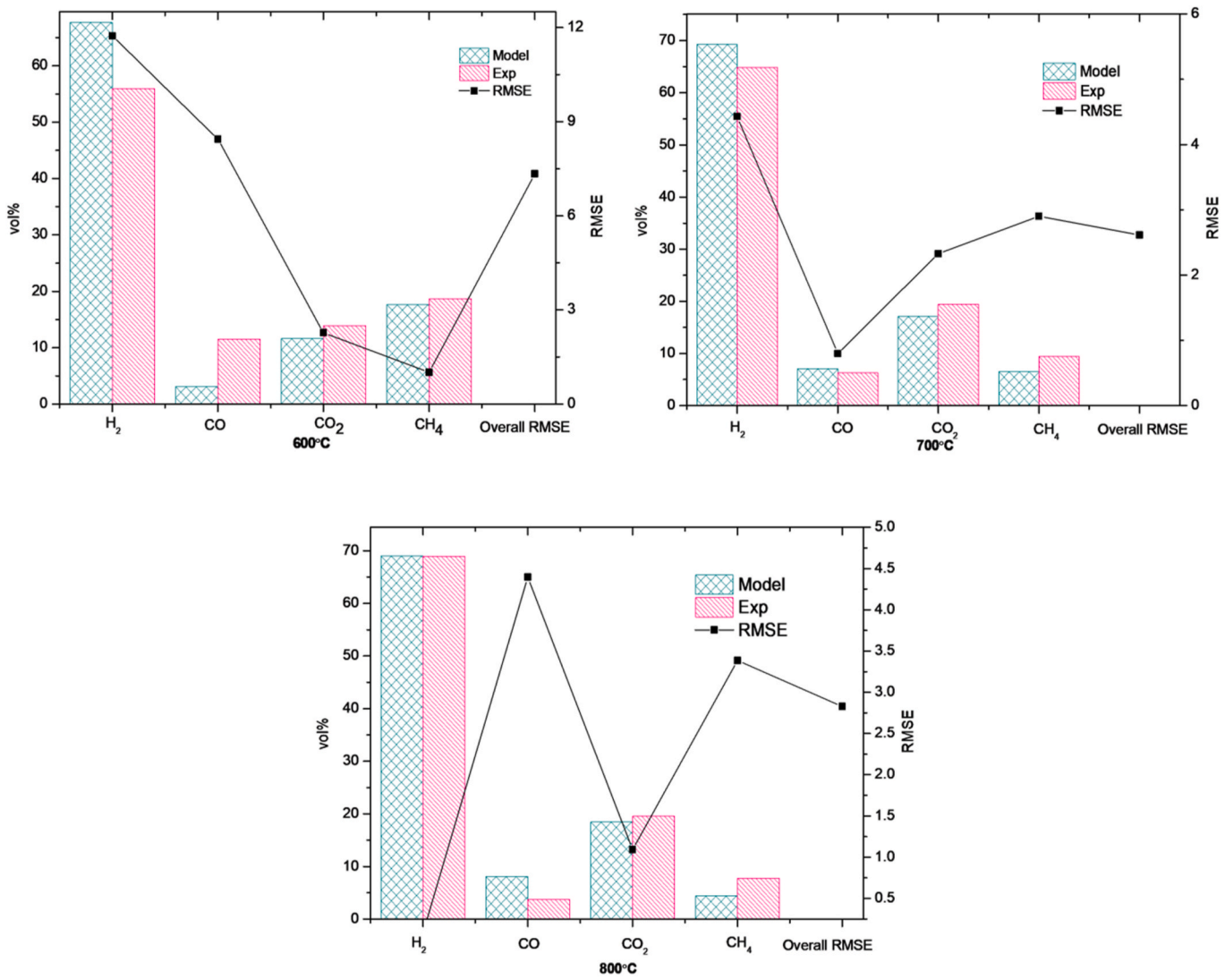

Fig. 7. RMSE validation results of the co-gasification at (a) 600 °C (b) 700 °C(c) 800 °C, CaO/F ratio = 1 and steam/feed ratio = 1.

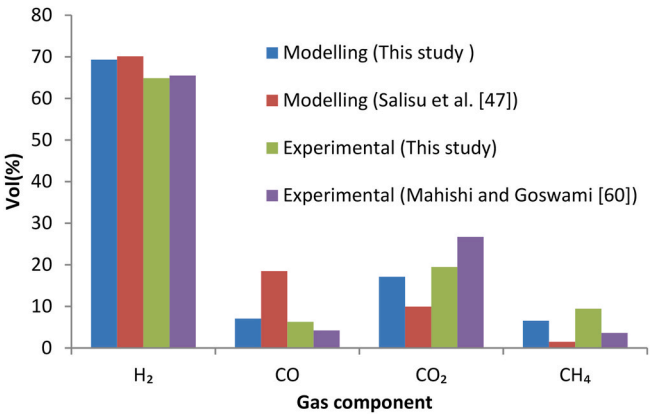

Fig. 8. Comparison of gas components (vol%) of the developed model with Salisu et al. [47], experimental data and pine bark gasification [60] at 700 °C.

Gasification with different feedstocks in the presence of CaO from previous studies also showed that maximum H_2 content is found at 670 °C [61], 680 °C [62], 700 °C [10,63], 780 °C [64]. It is important to note that under sorption-enhanced gasification conditions, temperature affects the thermodynamic equilibrium of both carbonation and calcination reactions [65]. CO_2 capture via carbonation reaction promotes water-gas shift reaction, hence more H_2 is produced. However, above 750 °C, calcination reaction seems to be prevailing, thereby reducing the concentration of H_2. Conversely, the content of CH_4 decreases with the increase in temperature; higher temperatures favour CH_4 reforming, hence this explains the observed trend of the CH_4 content. Both CO and CO_2 contents increase with the increasing temperature, their contents are largely influenced by the Boudouard (endothermic) and water gas shift (exothermic) reactions. A similar trend is observed on gas components in the literature [10,20,60,66]. Overall, the content of H_2, CO, CH_4 and CO_2 are largely dependent on the temperature, which also influences the sorption-enhanced gasification behaviour. Also from Fig. 9, the gas yield increases with the temperature from 1.46 Nm^3/kg at 600 °C to 2.40 Nm^3/kg at 850 °C. This is so because the conversion of char is enhanced at higher temperatures [61]. As on gas yield, the same effect is observed on CCE and CGE with values of 50.23–80.58% and 57.75–67.62%, respectively within the temperature range of 600–850 °C. However, on LHV of the gas, a negative trend is observed, where LHV decreases from 14.01 to 9.96 MJ/Nm^3. The reduction in the LHV is largely due to the consumption of CH_4 with the increase in temperature and CH_4 has the highest energy contribution in the syngas [8].

Depicted in Fig. 10 is the comparison between sorption and non-

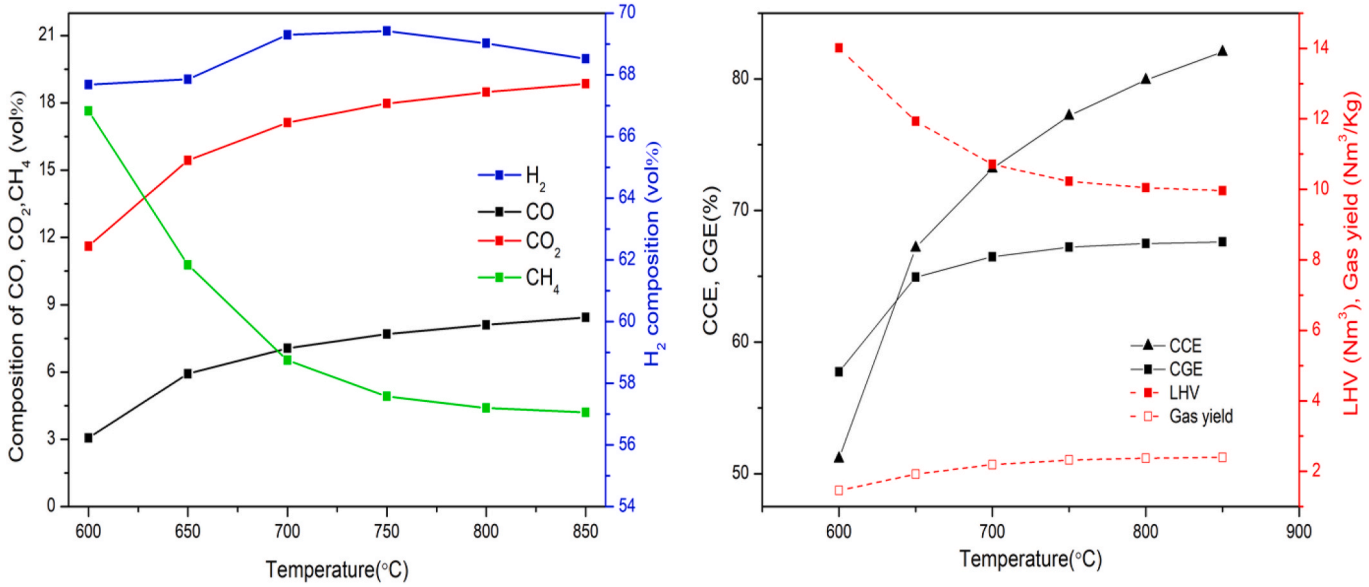

Fig. 9. Effects of temperature on co-gasification RH and LDPE at CaO/F ratio = 1 and steam/feed ratio = 1.

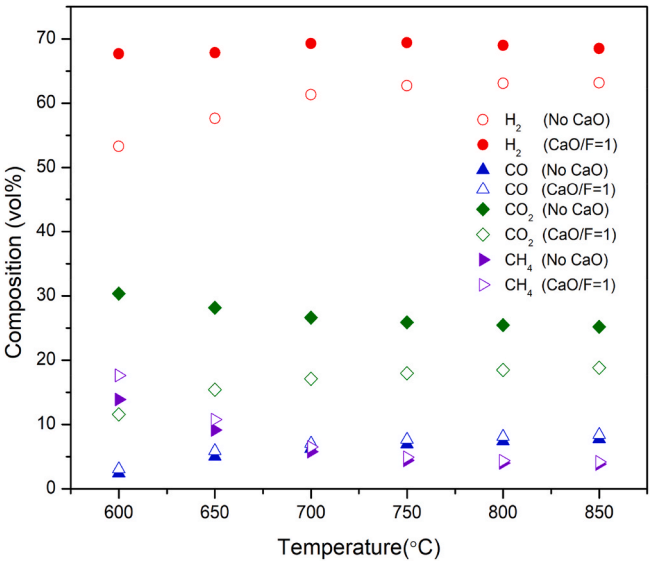

Fig. 10. Comparison between sorption and non-sorption gasification at different temperatures at steam/feed ratio = 1.

sorption gasification at different temperatures. At 600 °C, H_2 and CO_2 contents are 53.31 vol% and 30.38 vol%, for the sorption-enhanced gasification and 67.69 vol% and 11.61 vol%, for the non-sorption gasification. Similarly, at 850 °C, H_2 and CO_2 contents are 63.17 vol% and 25.19 vol%, for the sorption-enhanced gasification and 68.52 vol% and 18.84 vol%, for the non-sorption gasification. It is obvious that the sorption-enhanced gasification is more enhanced at lower temperature than at higher temperature. Similar observation was made by Mahishi and Goswami [60] work.

3.3.2. Steam/feed ratio

In gasification, steam is used as a gasifying agent to increase the H_2 content, hence, the variation of steam-to-feed ratio between 0.75 and 1.75 was examined in this simulation. As shown in Fig. 11, at 700 °C and CaO/F ratio = 1, increasing steam/feed leads to an increase in H_2 from 64.43 vol% to 74.88 vol%, while the content of CO reduces from 15.38 vol% to 3.16 vol%. This is so because increasing steam supply in gasification enhances H_2 production according to water–gas shift and steam reforming reactions [67]. Thus, the same trend as on CO content is observed with CH_4 content. On CO_2 content, an inconsistent trend is noticed [65], its content first increases between steam/feed ratio of 0.75 and 1.0. On the contrary, between steam/feed ratio of 1.0 and 1.5, CO_2 content reduces from 17.11 vol% to 15.27 vol%. Further increase in the steam/feed ratio resulted to increase in CO_2 content as 16.61 vol%. Suggesting that at steam/feed ratio = 1.0–1.5, CO_2 consumed by sorption-enhanced gasification is dominant over CO_2 produced as a result of steam injection [67]. Beyond steam/feed ratio of 1.5, excess steam might have affected the CO_2 sorption efficiency Mahishi and Goswami [60] explained that CO_2 is produced in the product gas in three ways: from biomass/plastic direct decomposition, tars/hydrocarbons cracking in the presence of steam and water–gas shift reaction.

Further analysis showed that increasing the steam supply causes both CCE and CGE to reduce monotonically from 79.05% to 59.64% and 73.00% to 51.94%, respectively. This trend is also established in the literature [68]. Similarly, LHV of the gas reduces from 11.24 to 10.54 MJ/Nm^3, however, gas yield increases from 2.04 to 2.22 Nm^3/kg. On CGE, it means that with higher steam, H_2 energy gained could not compensate for the energy associated with the steam. On CCE and LHV, loss of carbon content in the syngas in form of CO and CH_4 is responsible for the observed trend [10].

3.3.3. CaO/feed ratio

The addition of CaO in gasification is mainly to reduce the concentration of CO_2 and increase that of H_2 through carbonation reaction and enhancement of water-gas shift reaction [69]. From Fig. 12, the effect of CaO/F ratio is analyzed. An increase in CaO/F ratio from 0.25 to 1.0 increases H_2 concentration from 63.94% to 69.33% at 700 °C. The content of CO_2 reduces from 23.55% at CaO/F ratio of 0.25 to 17.11% at CaO/F ratio of 1.0. The impact of variation of CaO/F ratio between 0.25 and 1.0 is noticeable on CCE, which reduces from 85.50% to 71.89%. The decreasing trend observed is due to the reduction of carbon content in the syngas, which is caused by CO_2 capture [10]. On the other hand, CGE remains almost unchanged and this result is consistent with that of Kumari et al. [8]. On LHV, an increase from 9.88 to 10.71 MJ/Nm^3 is observed with the increasing CaO/F ratio, which is due to the increase in H_2 content [10], gas yield, however, reduces from 2.38 to 2.19 Nm^3/kg.

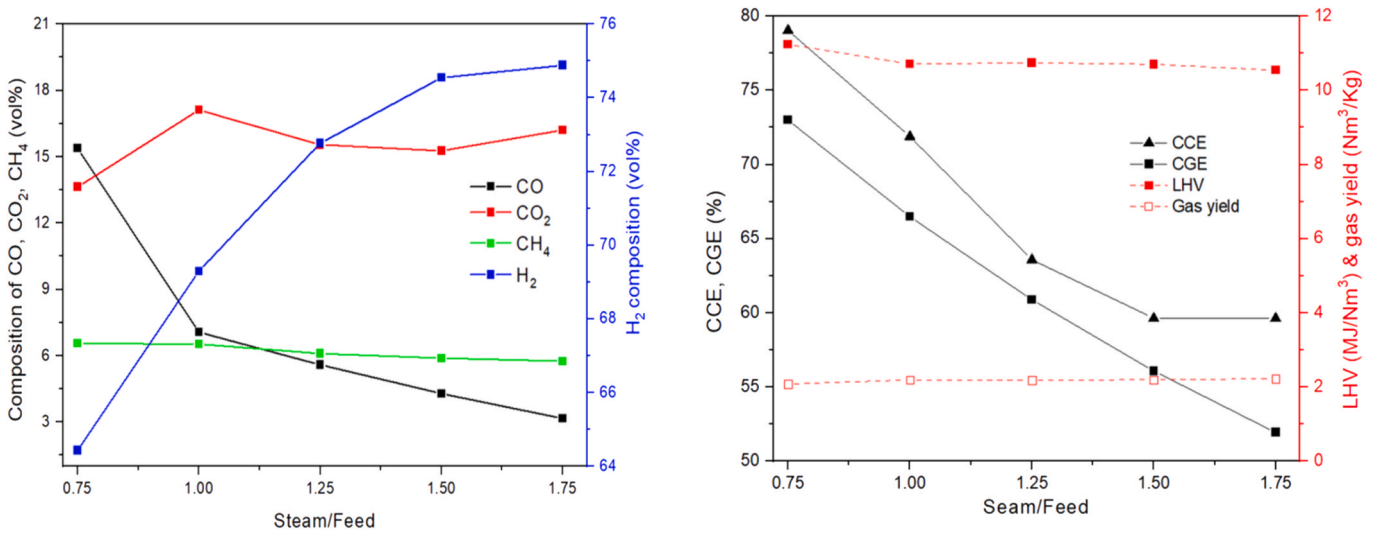

Fig. 11. Effects of steam/feed ratio on co-gasification of RH and LDPE at CaO/F ratio = 1 and 700 °C.

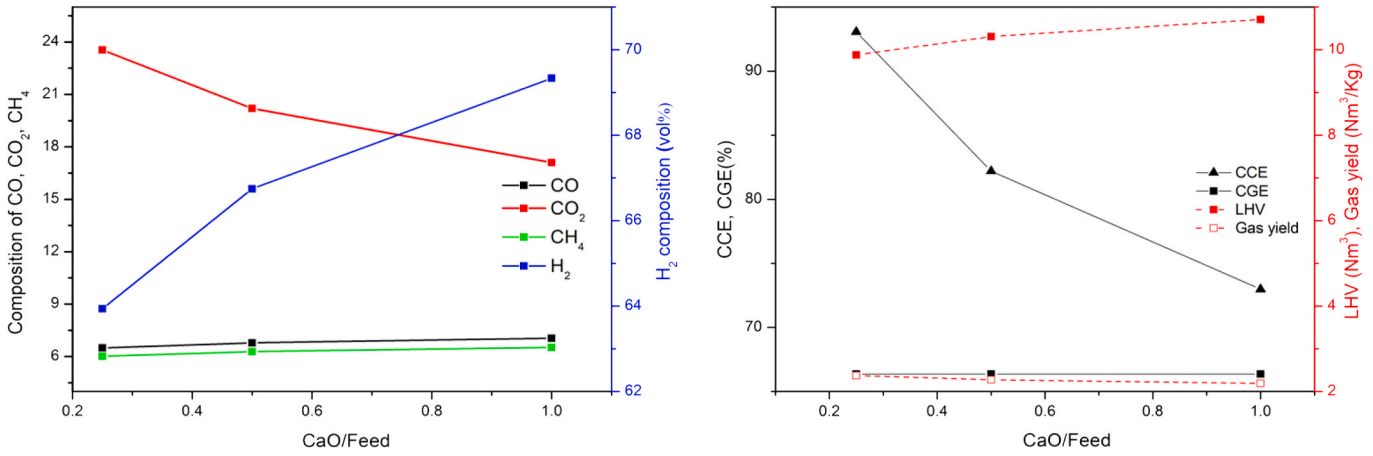

Fig. 12. Effects of CaO/F ratio on co-gasification of RH and LDPE at steam/feed ratio = 1 and 700 °C.

4. Conclusions

A novel Aspen Plus simulation for co-gasification of rice husk (RH) and plastic with an integrated ANN model for H_2 production was developed. The ANN model was used to predict the pyrolysis process involved in gasification. The ANN model development and its application for predicting new pyrolysis products were successful with correlation coefficient (R) values between 0.979 and 0.998. In addition, the least values in terms of performance were obtained as 1.639, 2.247 and 0.196, respectively for absolute error (MAE), root mean square error (RMSE) and mean bias error (MBE). The Aspen Plus simulation results showed that between 600 and 850 °C, the maximum H_2 content is obtained as 69.42 vol% at 750 °C. Temperature had a positive influence on gas yield, cold gasification efficiency (CGE) and carbon conversion efficiency (CCE) but with a negative effect on the lower heating value (LHV) of the syngas. Increasing steam/feed ratio increases H_2 content but decreases CO content of the syngas. Both CGE and CCE were influenced negatively by increasing steam/feed ratio. The validation of the Aspen Plus gasification simulation with experimental data at 600–800 °C gives RMSE values between 7.34 and 2.62, with the best value at 700 °C. Overall, a new approach was developed for future applications in the simulation of gasification. In addition, using the weight and biases results of the ANN model obtained in this study, pyrolysis products of biomass or plastic can be predicted. The required inputs will be the new ultimate analysis, pyrolysis temperature, and higher heating value (HHV).

Declaration of competing interest

The authors declare that they have no known competing financial interests or personal relationships that could have appeared to influence the work reported in this paper.

Acknowledgement

The authors would like to appreciate the National Natural Science Foundation of China (No. 52276211), Science and Technology Exchange Project of China Ministry of Science and Technology (No.2021-12-2), Education Cooperation Project between China and Central Eastern European Countries from China Education Association for International Exchange (No. 2021086), and PhD study sponsorship of Mr Salisu by Petroleum Technology Development Fund, Nigeria (PTDF/ED/PHD/PJS/33/18).

Appendix A. Supplementary data

Supplementary data to this article can be found online at https://doi.org/10.1016/j.joei.2023.101239.

References

[1] M. Irfan, A. Li, L. Zhang, M. Javid, M. Wang, S. Khushk, Enhanced H_2 production from municipal solid waste gasification using Ni-CaO-TiO_2 bifunctional catalyst prepared by dc arc plasma melting, Ind. Eng. Chem. Res. (2019), https://doi.org/10.1021/acs.iecr.9b01999.

[2] L. Dong, C. Wu, H. Ling, J. Shi, P.T. Williams, J. Huang, Development of Fe-promoted Ni–Al catalysts for hydrogen production from gasification of wood sawdust, Energy Fuels 31 (2017) 2118–2127, https://doi.org/10.1021/acs.energyfuels.6b02050.

[3] N. Gao, K. Kamran, C. Quan, P.T. Williams, Thermochemical conversion of sewage sludge: a critical review, Prog. Energy Combust. Sci. (2020), https://doi.org/10.1016/j.pecs.2020.100843.

[4] N. Gao, J. Salisu, C. Quan, P. Williams, Modified nickel-based catalysts for improved steam reforming of biomass tar: a critical review, Renew. Sustain. Energy Rev. (2021), https://doi.org/10.1016/j.rser.2021.111023.

[5] A.C. Dyer, M.A. Nahil, P.T. Williams, Catalytic co-pyrolysis of biomass and waste plastics as a route to upgraded bio-oil, J. Energy Inst. (2021), https://doi.org/10.1016/j.joei.2021.03.022.

[6] UNEP, Single-Use Plastic, A Roadmap for Sustainability, 2018.

[7] S. Chen, Z. Zhao, A. Soomro, S. Ma, M. Wu, Z. Sun, W. Xiang, Hydrogen-rich Syngas Production via Sorption-Enhanced Steam Gasification of Sewage Sludge, Biomass and Bioenergy, 2020, https://doi.org/10.1016/j.biombioe.2020.105607.

[8] P. Kumari, B. Mohanty, Hydrogen-rich gas production with CO_2 capture from steam gasification of pine needle using calcium oxide: experimental and modeling study, Int. J. Energy Res. (2020), https://doi.org/10.1002/er.5455.

[9] T. Detchusananard, K. Im-orb, P. Ponpesh, A. Arpornwichanop, Biomass gasification integrated with CO_2 capture processes for high-purity hydrogen production: process performance and energy analysis, Energy Convers. Manag. (2018), https://doi.org/10.1016/j.enconman.2018.06.072.

[10] M. Shahbaz, S. Yusup, A. Inayat, M. Ammar, D.O. Patrick, A. Pratama, S.R. Naqvi, Syngas Production from Steam Gasification of Palm Kernel Shell with Subsequent CO_2 Capture Using CaO Sorbent: an Aspen Plus Modeling, Energy and Fuels, 2017, https://doi.org/10.1021/acs.energyfuels.7b02670.

[11] B. Li, C. Fabrice Magoua Mbeugang, D. Liu, S. Zhang, S. Wang, Q. Wang, Z. Xu, X. Hu, Simulation of sorption enhanced staged gasification of biomass for hydrogen production in the presence of calcium oxide, Int. J. Hydrogen Energy (2020), https://doi.org/10.1016/j.ijhydene.2020.07.121.

[12] M. Fernandez-Lopez, J. Pedroche, J.L. Valverde, L. Sanchez-Silva, Simulation of the gasification of animal wastes in a dual gasifier using Aspen Plus, Energy Convers. Manag. 140 (2017) 211–217, https://doi.org/10.1016/J.ENCONMAN.2017.03.008.

[13] V. Marcantonio, E. Bocci, D. Monarca, Development of a chemical quasi-equilibrium model of biomass waste gasification in a fluidized-bed reactor by using Aspen plus, Energies (2019), https://doi.org/10.3390/en13010053.

[14] L.E. Arteaga-Pérez, Y. Casas-Ledón, R. Pérez-Bermúdez, L.M. Peralta, J. Dewulf, W. Prins, Energy and exergy analysis of a sugar cane bagasse gasifier integrated to a solid oxide fuel cell based on a quasi-equilibrium approach, Chem. Eng. J. (2013), https://doi.org/10.1016/j.cej.2013.05.077.

[15] M.C. Acar, Y.E. Böke, Simulation of Biomass Gasification in a BFBG Using Chemical Equilibrium Model and Restricted Chemical Equilibrium Method, Biomass and Bioenergy, 2019, https://doi.org/10.1016/j.biombioe.2019.04.012.

[16] G. Mirmoshtaghi, H. Li, E. Thorin, E. Dahlquist, Evaluation of Different Biomass Gasification Modeling Approaches for Fluidized Bed Gasifiers, Biomass and Bioenergy, 2016, https://doi.org/10.1016/j.biombioe.2016.05.002.

[17] M. Fernandez-Lopez, J. Pedroche, J.L. Valverde, L. Sanchez-Silva, Simulation of the gasification of animal wastes in a dual gasifier using Aspen Plus, Energy Convers. Manag. (2017), https://doi.org/10.1016/j.enconman.2017.03.008.

[18] T. Detchusananard, P. Ponpesh, D. Saebea, S. Authayanun, A. Arpornwichanop, Modeling and analysis of sorption enhanced chemical looping biomass gasification, Chem. Eng. Trans. (2017), https://doi.org/10.3303/CET1757018.

[19] T. Detchusananard, K. Im-orb, F. Maréchal, A. Arpornwichanop, Analysis of the sorption-enhanced chemical looping biomass gasification process: performance assessment and optimization through design of experiment approach, Energy (2020), https://doi.org/10.1016/j.energy.2020.118190.

[20] S. Rupesh, C. Muraleedharan, P. Arun, ASPEN plus modelling of air–steam gasification of biomass with sorbent enabled CO_2 capture, Resour. Technol. (2016), https://doi.org/10.1016/j.reffit.2016.07.002.

[21] E. Ansah, Experimental Investigation and A Spen Plus Simulation of the, MSW Pyrolysis, 2013.

[22] S. Safarian, S.M. Ebrahimi Saryazdi, R. Unnthorsson, C. Richter, Artificial neural network integrated with thermodynamic equilibrium modeling of downdraft biomass gasification-power production plant, Energy (2020), https://doi.org/10.1016/j.energy.2020.118800.

[23] H. Li, Z. Zhang, Z. Liu, Application of artificial neural networks for catalysis: a review, Catalysts (2017), https://doi.org/10.3390/catal7100306.

[24] D. Baruah, D.C. Baruah, M.K. Hazarika, Artificial Neural Network Based Modeling of Biomass Gasification in Fixed Bed Downdraft Gasifiers, Biomass and Bioenergy, 2017, https://doi.org/10.1016/j.biombioe.2017.01.029.

[25] Y. Sun, L. Liu, Q. Wang, X. Yang, X. Tu, Pyrolysis products from industrial waste biomass based on a neural network model, J. Anal. Appl. Pyrolysis (2016), https://doi.org/10.1016/j.jaap.2016.04.013.

[26] D. Serrano, D. Castelló, Tar prediction in bubbling fluidized bed gasification through artificial neural networks, Chem. Eng. J. (2020), https://doi.org/10.1016/j.cej.2020.126229.

[27] S. Sunphorka, B. Chalermsinsuwan, P. Piumsomboon, Artificial neural network model for the prediction of kinetic parameters of biomass pyrolysis from its constituents, Fuel (2017), https://doi.org/10.1016/j.fuel.2016.12.046.

[28] D. Cerinski, J. Baleta, H. Mikulčić, R. Mikulandrić, J. Wang, Dynamic modelling of the biomass gasification process in a fixed bed reactor by using the artificial neural network, Clean. Eng. Technol. (2020), https://doi.org/10.1016/j.clet.2020.100029.

[29] R. Mikulandrić, D. Lončar, D. Böhning, R. Böhme, M. Beckmann, Artificial neural network modelling approach for a biomass gasification process in fixed bed gasifiers, Energy Convers. Manag. (2014), https://doi.org/10.1016/j.enconman.2014.03.036.

[30] A.Y. Mutlu, O. Yucel, An artificial intelligence based approach to predicting syngas composition for downdraft biomass gasification, Energy (2018), https://doi.org/10.1016/j.energy.2018.09.131.

[31] D.S. Pandey, S. Das, I. Pan, J.J. Leahy, W. Kwapinski, Artificial neural network based modelling approach for municipal solid waste gasification in a fluidized bed reactor, Waste Manag. (2016), https://doi.org/10.1016/j.wasman.2016.08.023.

[32] H. Wang, L.A. Ricardez-Sandoval, Dynamic optimization of a pilot-scale entrained-flow gasifier using artificial recurrent neural networks, Fuel (2020), https://doi.org/10.1016/j.fuel.2020.117731.

[33] M. Shahbaz, S.A. Taqvi, A.C. Minh Loy, A. Inayat, F. Uddin, A. Bokhari, S.R. Naqvi, Artificial neural network approach for the steam gasification of palm oil waste using bottom ash and CaO, Renew. Energy (2019), https://doi.org/10.1016/j.renene.2018.07.142.

[34] J. Chen, J. Liu, Y. He, L. Huang, S. Sun, J. Sun, K.L. Chang, J. Kuo, S. Huang, X. Ning, Investigation of co-combustion characteristics of sewage sludge and coffee grounds mixtures using thermogravimetric analysis coupled to artificial neural networks modeling, Bioresour. Technol. (2017), https://doi.org/10.1016/j.biortech.2016.11.069.

[35] D.M. Himmelblau, Applications of Artificial Neural Networks in Chemical Engineering, Korean J. Chem. Eng., 2000, https://doi.org/10.1007/BF02706848.

[36] M. Ozonoh, B.O. Oboirien, A. Higginson, M.O. Daramola, Performance evaluation of gasification system efficiency using artificial neural network, Renew. Energy (2020), https://doi.org/10.1016/j.renene.2019.07.136.

[37] S.K. Arumugasamy, A. Selvarajoo, M.A. Tariq, Artificial neural networks modelling: gasification behaviour of palm fibre biochar, Mater. Sci. Energy Technol. (2020), https://doi.org/10.1016/j.mset.2020.10.010.

[38] A.I. Lawal, M.A. Idris, An artificial neural network-based mathematical model for the prediction of blast-induced ground vibrations, Int. J. Environ. Stud. (2020), https://doi.org/10.1080/00207233.2019.1662186.

[39] A. Dewangan, D. Pradhan, R.K. Singh, Co-pyrolysis of sugarcane bagasse and low-density polyethylene: influence of plastic on pyrolysis product yield, Fuel (2016), https://doi.org/10.1016/j.fuel.2016.08.011.

[40] H.S. Heo, H.J. Park, J.I. Dong, S.H. Park, S. Kim, D.J. Suh, Y.W. Suh, S.S. Kim, Y. K. Park, Fast pyrolysis of rice husk under different reaction conditions, J. Ind. Eng. Chem. (2010), https://doi.org/10.1016/j.jiec.2010.01.026.

[41] O. Senneca, T. Tucciullo, Lumped kinetics for homogeneous reactions of n-hexadecane and n-decene as model compounds for pe pyrolysis primary tars, Energies (2020), https://doi.org/10.3390/en13205466.

[42] B. Ciuffi, D. Chiaramonti, A.M. Rizzo, M. Frediani, L. Rosi, A critical review of SCWG in the context of available gasification technologies for plastic waste, Appl. Sci. (2020), https://doi.org/10.3390/APP10186307.

[43] T. Damartzis, S. Michailos, A. Zabaniotou, Energetic assessment of a combined heat and power integrated biomass gasification-internal combustion engine system by using Aspen Plus®, Fuel Process, Technol. (2012), https://doi.org/10.1016/j.fuproc.2011.11.010.

[44] W. Lan, G. Chen, X. Zhu, X. Wang, C. Liu, B. Xu, Biomass gasification-gas turbine combustion for power generation system model based on ASPEN PLUS, Sci. Total Environ. (2018), https://doi.org/10.1016/j.scitotenv.2018.02.159.

[45] M. Formica, S. Frigo, R. Gabbrielli, Development of a new steady state zero-dimensional simulation model for woody biomass gasification in a full scale plant, Energy Convers. Manag. (2016), https://doi.org/10.1016/j.enconman.2016.05.009.

[46] L.P.R. Pala, Q. Wang, G. Kolb, V. Hessel, Steam gasification of biomass with subsequent syngas adjustment using shift reaction for syngas production: an Aspen Plus model, Renew. Energy (2017), https://doi.org/10.1016/j.renene.2016.08.069.

[47] J. Salisu, N. Gao, C. Quan, Techno-economic assessment of Co-gasification of rice husk and plastic waste as an off-grid power source for small scale rice milling - an aspen plus model, J. Anal. Appl. Pyrolysis (2021), https://doi.org/10.1016/j.jaap.2021.105157.

[48] N.S. Barman, S. Ghosh, S. De, Gasification of biomass in a fixed bed downdraft gasifier - a realistic model including tar, Bioresour. Technol. (2012), https://doi.org/10.1016/j.biortech.2011.12.124.

[49] I.L. Motta, A.N. Marchesan, R. Maciel Filho, M.R. Wolf Maciel, Correlating biomass properties, gasification performance, and syngas applications of Brazilian feedstocks via simulation and multivariate analysis, Ind. Crop. Prod. (2022), https://doi.org/10.1016/j.indcrop.2022.114808.

[50] S. Sezer, F. Kartal, U. Özveren, Artificial intelligence approach in gasification integrated solid oxide fuel cell cycle, Fuel (2022), https://doi.org/10.1016/j.fuel.2021.122591.

[51] F. Abnisa, S.D.A. Sharuddin, M.F. bin Zanil, W.M.A.W. Daud, T.M.I. Mahlia, The yield prediction of synthetic fuel production from pyrolysis of plasticwaste by Levenberg-Marquardt approach in feedforward neural networks model, Polymers (2019), https://doi.org/10.3390/polym11111853.

[52] I. Dubdub, M. Al-Yaari, Pyrolysis of mixed plastic waste: ii. artificial neural networks prediction and sensitivity analysis, Appl. Sci. (2021), https://doi.org/10.3390/app11188456.
[53] D. Nettleton, Selection of variables and factor derivation, in: Commer. Data Min., Elsevier, 2014, pp. 79–104, https://doi.org/10.1016/b978-0-12-416602-8.00006-6.
[54] M. Theristis, V. Venizelou, G. Makrides, G.E. Georghiou, Energy yield in photovoltaic systems, in: McEvoy's Handb. Photovoltaics Fundam. Appl., 2018, pp. 671–713, https://doi.org/10.1016/B978-0-12-809921-6.00017-3.
[55] Y. Yu, Y. Yang, Z. Cheng, P.H. Blanco, R. Liu, A.V. Bridgwater, J. Cai, Pyrolysis of rice husk and corn stalk in auger reactor. 1. Characterization of char and gas at various temperatures, Energy Fuel. (2016), https://doi.org/10.1021/acs.energyfuels.6b02276.
[56] J.M. Encinar, F.J. Beltrán, J.F. González, M.J. Moreno, Pyrolysis of maize, sunflower, grape and tobacco residues, J. Chem. Technol. Biotechnol. (1997), https://doi.org/10.1002/(SICI)1097-4660(199712)70:4<400::AID-JCTB797>3.0.CO;2-6.
[57] X. Wang, S.R.A. Kersten, W. Prins, W.P.M. Van Swaaij, Biomass pyrolysis in a fluidized bed reactor. Part 2: experimental validation of model results, Ind. Eng. Chem. Res. (2005), https://doi.org/10.1021/ie050486y.
[58] N. Gautam, A. Chaurasia, Study on kinetics and bio-oil production from rice husk, rice straw, bamboo, sugarcane bagasse and neem bark in a fixed-bed pyrolysis process, Energy (2020), https://doi.org/10.1016/j.energy.2019.116434.
[59] X. Chen, H. Zhang, Y. Song, R. Xiao, Prediction of product distribution and bio-oil heating value of biomass fast pyrolysis, Chem. Eng. Process. - Process Intensif. (2018), https://doi.org/10.1016/j.cep.2018.05.018.
[60] M.R. Mahishi, D.Y. Goswami, An experimental study of hydrogen production by gasification of biomass in the presence of a CO_2 sorbent, Int. J. Hydrogen Energy (2007), https://doi.org/10.1016/j.ijhydene.2007.03.030.
[61] B. Acharya, A. Dutta, P. Basu, An investigation into steam gasification of biomass for hydrogen enriched gas production in presence of CaO, Int. J. Hydrogen Energy (2010), https://doi.org/10.1016/j.ijhydene.2009.11.109.
[62] M. Hussain, L.D. Tufa, S. Yusup, H. Zabiri, A kinetic-based simulation model of palm kernel shell steam gasification in a circulating fluidized bed using Aspen Plus®: a case study, Biofuels (2018), https://doi.org/10.1080/17597269.2018.1461510.
[63] G. Chen, F. Liu, X. Guo, Y. Zhang, B. Yan, Z. Cheng, L. Xiao, W. Ma, L. Hou, Co-gasification of Acid Hydrolysis Residues and Sewage Sludge in a Downdraft Fixed Gasifier with CaO as an In-Bed Additive, Energy and Fuels, 2018, https://doi.org/10.1021/acs.energyfuels.7b03960.
[64] Q. Wang, N. Rong, H. Fan, Y. Meng, M. Fang, L. Cheng, K. Cen, Enhanced hydrogen-rich gas production from steam gasification of coal in a pressurized fluidized bed with CaO as a CO_2 sorbent, in: Int. J. Hydrogen Energy, 2014, https://doi.org/10.1016/j.ijhydene.2014.01.153.
[65] J. Dong, A. Nzihou, Y. Chi, E. Weiss-Hortala, M. Ni, N. Lyczko, Y. Tang, M. Ducousso, Hydrogen-Rich Gas Production from Steam Gasification of Bio-Char in the Presence of CaO, Waste and Biomass Valorization, 2017, https://doi.org/10.1007/s12649-016-9784-x.
[66] A. Inayat, M.M. Ahmad, S. Yusup, M.I.A. Mutalib, Biomass steam gasification with in-situ CO_2 capture for enriched hydrogen gas production: a reaction kinetics modelling approach, Energies (2010), https://doi.org/10.3390/en3081472.
[67] L. Wei, H. Yang, B. Li, X. Wei, L. Chen, J. Shao, H. Chen, Absorption-enhanced steam gasification of biomass for hydrogen production: effect of calcium oxide addition on steam gasification of pyrolytic volatiles, Int. J. Hydrogen Energy (2014), https://doi.org/10.1016/j.ijhydene.2014.07.064.
[68] Z. Liu, C. Zhao, L. Cai, X. Long, Steady state modelling of steam-gasification of biomass for H_2-rich syngas production, Energy (2022), https://doi.org/10.1016/j.energy.2021.121616.
[69] L. Wei, S. Xu, J. Liu, C. Liu, S. Liu, Hydrogen Production in Steam Gasification of Biomass with CaO as a CO_2 Absorbent, Energy and Fuels, 2008, https://doi.org/10.1021/ef700744a.